Analytic representation for first-principles pseudopotentials

Pui K. Lam and Marvin L. Cohen
Department of Physics, University of California, Berkeley, California 94720
and Materials and Molecular Research Division, Lawrence Berkeley Laboraotry, Berkeley, California 94720

Alex Zunger
Solar Energy Research Institute, Golden, Colorado 80401
(Received 18 January 1980)

The first-principles pseudopotentials developed by Zunger and Cohen are fit with a simple analytic form chosen to model the main physical properties of the potentials. The fitting parameters for the first three rows of the Periodic Table are presented, and the quality of the fit is discussed. The parameters reflect chemical trends of the elements. We find that a minimum of three parameters is required to reproduce the regularities of the Periodic Table. Application of these analytic potentials is also discussed.

INTRODUCTION

It is well known that pseudopotentials do not have a unique representation. The general requirement of a pseudopotential is that it reproduce the valence characteristics of an all-electron system. Zunger and Cohen[1] have developed a systematic method to produce pseudopotentials in the density-functional (DF) formalism for any element in the Periodic Table by imposing certain physically motivated constraints on the pseudo-wave-functions. The Zunger-Cohen potentials were successfully applied to characterize a large class of crystal structures[2] and were applied to a number of electronic structure problems (e.g., bulk properties[3]). However, these potentials are given in numerical form and, hence, are not easily accessible. In this work, an analytic form is used to fit the potentials. This form is given by Eq. (29), and the fitting parameters are tabulated in Tables I–IV and the Appendix. The form chosen is simple so that the physical properties of the potentials could become more apparent. In Sec. I the choice of the analytic form and its physical interpretation are discussed. In Sec. II the calculational methods are described, and in Sec. III the quality of the fits are discussed. Section IV describes the chemical trends reflected by the fitting parameters; applications of these analytic potentials are also briefly discussed.

I. ANALYTIC FORM OF THE PSEUDOPOTENTIAL

The formalism of Ref. 1 has been implemented by using numerical integrations, and the resulting pseudopotentials are, thus, numerical. They can be used in numerical form for electronic-structure calculation[1-3]; however, in this paper, we are concerned primarily with simple, analytical representations which reproduce in a transparent form the systematics of the potentials. We will, therefore, start from the exact closed form of the potential and apply a number of simplifying approximations to deduce the correct analytical asymptotic forms. We will then use these forms to devise a simple interpolative analytic form for all r values.

The exact expression for the Zunger-Cohen potential of a particular angular momentum symmetry, l, is[1]

$$V_{ps}^{l}(r) = U_l(r) + V_T[\rho] - V_V[n] . \tag{1}$$

$U_l(r)$ is the nonlocal (i.e., l-dependent) "Pauli-force" term which replaces the kinetic energy of the true valence state, due to valence-core orthogonality, by a potential barrier. $U_l(r)$ has the following closed form[1]:

$$U_l(r) = \frac{\sum_n^V C_{nl}(\epsilon_{Nl} - \epsilon_{nl})\psi_{nl}(r)}{\sum_n^N C_{nl}\psi_{nl}(r)} . \tag{2}$$

The ψ_{nl}'s are the all-electron nodal wave functions (i.e., core and valence) and ϵ_{nl}'s are the corresponding eigenvalues. N is the principal quantum number of the valence state for which the potential is generated, and the sum is extended over both the core and valence states. The C_{nl}'s define the normalized pseudo-wave-function, $\chi_{Nl}(r)$, through the unitary rotation

$$\chi_{Nl}(r) \equiv \sum_n^N C_{nl}\psi_{nl}(r) . \tag{3}$$

In the Zunger-Cohen scheme, the C_{nl}'s are determined by imposing some physically motivated constraints on $\chi_{Nl}(r)$.[1] Generally, $C_{Nl} \simeq 1$ and $C_{nl} \ll 1$ for the core; i.e., χ_{Nl} is mostly valence in character with a small admixture of core states. Note that in Eq. (2), although the numerator is summed over both the core and valence states, the term $(\epsilon_{Nl} - \epsilon_{nl})$ makes the valence contribution

identically zero. Hence, if there is no core state for that particular l, then $U_l(r)$ is zero. This is in accord with Phillips's cancellation theorem[4] and the Pauli-force concept.[5] The functions $V_T[\rho]$ and $V_V[n]$ represent the local parts of the potential (i.e., common to all l's); their closed forms are

$$V_T[\rho] = -Z/r + V_{HX}[\rho] \tag{4}$$

and

$$V_V[n] = -Z_v/r + V_{HX}[n], \tag{5}$$

where Z is the atomic charge and Z_v is the valence charge.

The functions, $\rho(r)$ and $n(r)$, which are the all-electron core (c) plus valence (v) charge density and the pseudovalence charge density of the reference state,[6] are defined as

$$\rho(r) \equiv \sum_{n,l} |\psi_{nl}|^2 N_{nl}^{c,v} \tag{6}$$

and

$$n(r) \equiv \sum_{n,l} |\chi_{nl}|^2 N_{nl}^{v}, \tag{7}$$

where $N_{nl}^{c,v}$ and $N_{n,l}^{v}$ are the occupation numbers for the core-plus-valence and for the valence orbitals, respectively. V_{HX} is the self-consistent screening potential; in the Zunger-Cohen scheme, a local density functional is used for both the interelectronic Coulomb (Hartree) potential and the exchange potential with $\alpha = \frac{2}{3}$. When $V_{ps}^{l}(r)$ is used in the Schrödinger equation,

$$\left(-\tfrac{1}{2}\nabla^2 + \sum_l V_{ps}^{l}(r)\hat{P}_l + V_V[n]\right)\chi_{Nl}(r) = \lambda_{Nl}\chi_{Nl}(r), \tag{8}$$

where $\hat{P}_l$ is the angular momentum projection operator, $\sum_m |lm\rangle\langle ml|$, the valence eigenvalues are reproduced; i.e., $\lambda_{Nl} = \epsilon_{Nl}$.[1] Following the notation of Ref. 1, we will define the atomic core potential (or ionic potential) $W_l(r)$ as the sum of $V_{ps}^{l}(r)$ and $-Z_v/r$; i.e.,

$$W_l(r) \equiv V_{ps}^{l}(r) - Z_v/r. \tag{9}$$

The various components of the core potential for Sb, as obtained in the unapproximated numerical form, are depicted in Fig. 1. Curve 4 in Fig. 1 shows the typical shape of $W_l(r)$. $W_l(r)$ is characterized by a classical turning point, R_0^l,

$$W_l(R_0^l) \equiv 0 \tag{10}$$

and by a minimum point, R_m^l,

$$\left.\frac{dW_l}{dr}\right|_{R_m^l} \equiv 0. \tag{11}$$

We now examine the analytic properties of the various components of $W_l(r)$. Starting with the

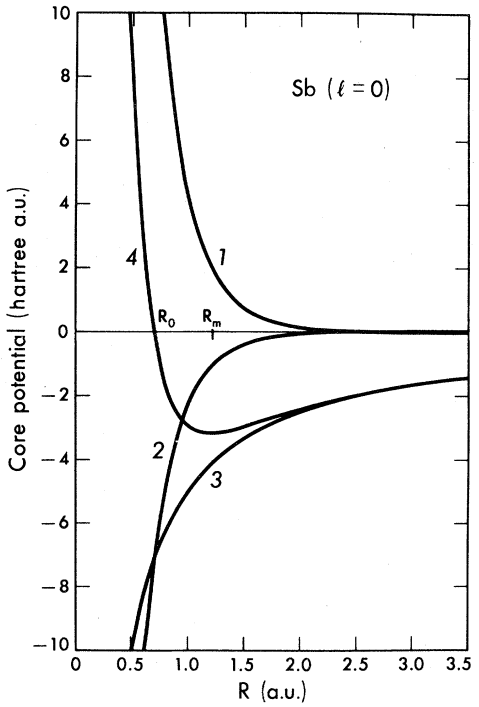

FIG. 1. Different contributions to the core (ionic) potential. (1) Pauli term; (2) core-screening term $= V_T - V_V$; (3) $-Z_v/r$; and (4) core potential, $W_l(r)$ = (1) + (2) + (3). The $l = 0$ Sb potential is used as an example.

Pauli term, as $r \to 0$, $U_l(r) \to C/r^2$. This results from the constraint imposed by the Zunger-Cohen scheme on the small-r expansion of the pseudo-wave-function[1]; $\lim_{r\to 0}\chi_{Nl}(r) = a_0 r^{l+\lambda} + \cdots$ with $\lambda = 2$.[7] Hence, at small r, $U_l(r)$ has the same form as the Pauli-force potential postulated by Simons and Bloch.[5] At large r, $U_l(r)$ diminishes very rapidly, tending to zero outside the core region (cf. curve 1 in Fig. 1). From Eq. (2) we note that, at large r, the dominant term in the numerator comes from the outermost core state and the denominator from the valence state. Since both of these states have an approximate exponential decay in this region, $U_l(r)$ also tends to zero exponentially. In the intermediate region $U_l(r)$ may have structure (cf. Fig. 2). In our fitting, for simplicity we approximate the Pauli term by

$$U_l^{\text{fit}}(r) = (C_1^l/r^2)\exp(-C_2^l r). \tag{12}$$

This has the same form as the "renormalized Pauli-force" potential of Andreoni *et al.*,[8] but here we see a microscopic justification of this form.

The local parts of the pseudopotential also have a simple physical interpretation. Combining V_T and V_V,

$$V_T(r) - V_V(r) = -Z_c/r + V_{HX}[\rho] - V_{HX}[n], \tag{13}$$

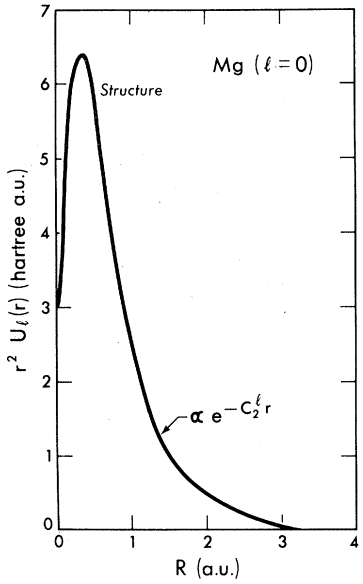

FIG. 2. Structure of the Pauli term in the core region.

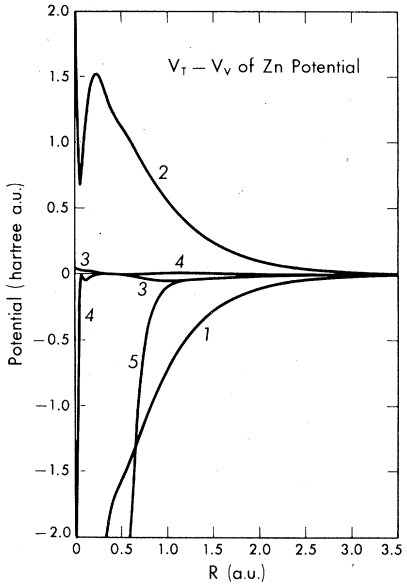

FIG. 3. Different contributions to the core-screening term, $V_T - V_V$. (1) $-Z_c/r + V_H[\rho_c] + V_X[\rho_c]$; (2) $V_X[\rho_c+\rho_v] - V_X[\rho_c] - V_X[\rho_v]$; (3) $V_H[\rho_v] - V_H[n]$; (4) $V_X[\rho_v] - V_X[n]$; and (5) $V_T - V_V$ = (1) + (2) + (3) + (4). $V_{\Delta\psi}$ = (3) + (4).

where Z_c is the core charge and it is equal to Z minus Z_v. This term mainly represents the electrostatic screening of the nucleus by the core electrons. To see this more clearly, we separate the contribution to the all-electron charge density into two parts, one from the core and one from the valence state; i.e.,

$$\rho \equiv \rho_c + \rho_v , \tag{14}$$

and rewriting (13) by adding and subtracting terms and by using the fact that $V_H[\rho]$ is a linear functional of ρ leads to

$$\begin{aligned} V_T(r) - V_V(r) = {} & (-Z_c/r + V_H[\rho_c] + V_X[\rho_c]) \\ & + (V_X[\rho_c+\rho_v] - V_X[\rho_c] - V_X[\rho_v]) \\ & + (V_H[\rho_v] - V_H[n] + V_X[\rho_v] - V_X[n]) . \end{aligned} \tag{15}$$

The different contributions are separated by round parentheses and are plotted in Fig. 3 for Zn. The dominant term is $(-Z_c/r + V_H[\rho_c] + V_X[\rho_c])$, which can be identified as the electrostatic potential due to a nucleus of charge Z_c screened by the core electrons. We denote this term by I. The second term $(V_X[\rho_c+\rho_v] - V_X[\rho_c] - V_X[\rho_v])$ arises from the nonlinearity of the exchange potential, $V_X[\rho] \propto \rho^{1/3}$, and we denote this term by II. The third term $(V_H[\rho_v] - V_H[n] + V_X[\rho_v] - V_X[n])$ comes from the mismatch between the all-electron valence wave functions and pseudovalence wave function, and we denote this term by $V_{\Delta\psi}(r)$.

We now examine the asymptotic behavior of the potential in Eq. (15). At large r ($r \to 1.5$ a.u.) there is an almost complete cancellation between I and II (cf. curves 1 and 2 in Fig. 3). The cancellation can be shown analytically by examining the asymptotic form of these terms. At large r

$$(-Z_c/r + V_H[\rho_c] + V_X[\rho_c]) \to V_X[\rho_c] \tag{16}$$

because $V_H[\rho_c]$ cancels $-Z_c/r$. Substituting the functional form for $V_X[\rho]$ in II and using the fact that at large r $\rho_v \gg \rho_c$, one obtains

$$(V_X[\rho_c+\rho_v] - V_X[\rho_c] - V_X[\rho_v]) \to -V_X[\rho_c] + O(\rho_c/\rho_v^{2/3}) \tag{17}$$

which cancels with (16). Thus at large r

$$V_T(r) - V_V(r) \to (Z_c/r + V_H[\rho_c]) + V_{\Delta\psi}(r) . \tag{18}$$

At small r

$$V_T(r) - V_V(r) \to -Z_c/r . \tag{19}$$

To first order, we can approximate $V_T - V_V$ by a Fermi-Thomas screening term

$$V_T(r) - V_V(r) \sim -(Z_c/r)\exp(-C_3 r) . \tag{20}$$

Although this is a good approximation for the $-Z_c/r + V_H[\rho_c]$ part, it fails to account for $V_{\Delta\psi}(r)$; for $r \geq 1.5$ a.u., $V_T(r) - V_V(r) \to V_{\Delta\psi}(r)$ (cf. curves 3, 4, and 5 in Fig. 3). It is important to account for this term in the fit in this region because the valence wave functions have their largest amplitudes

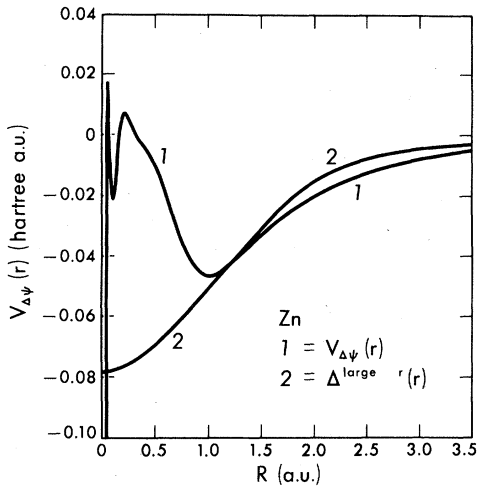

FIG. 4. Δ large $r(r)$ is a good fit for $V_{\Delta\psi}(r)$ at large r. Zn is used as an example.

at ~1–3 a.u. It turns out that the form

$$\Delta^{\text{large } r}(r)=\frac{-C_4C_5}{\pi^2(C_5^2+r^2)^2} \tag{21}$$

yields a good fit for $V_{\Delta\psi}(r)$ at large r (see Fig. 4).

The fit with the Fermi-Thomas term plus $\Delta^{\text{large } r}(r)$

$$V_T(r)-V_V(r)^{\text{fit}}=-(Z_c/r)\exp(-C_3r)+\Delta^{\text{large } r}(r) \tag{22}$$

works very well for atoms in the first two rows of the Periodic Table. However, for the third row (the transition metals), Eq. (22) is too attractive at small r. This is because, as Z increases and the core charge is pulled inward, the Fermi-Thomas form underscreens the nucleus. This effect can be accounted for by introducing

$$\Delta^{\text{small } r}(r)=C_6\exp(-C_7r). \tag{23}$$

This small-r correction is important for the $3d$ series because the d orbital is very localized. For example, using Eq. (22) for $V_T(r)-V_V(r)^{\text{fit}}$, the $3d$ pseudo-wave-function of Zn is pulled inward, and the $4s$ and $4p$ pseudo-wave-functions are pushed outward. The $4s$ and $4p$ orbitals are affected by the $3d$ orbitals through the self-consistent screening potential $V_{HX}[n]$. The eigenvalues are in error by 8–12%, but with the small-r correction included the error is ~1%. In our fitting procedure, the Ga to Br potentials are generated with the $3d$ shell in the core. There is no need to include the small-r correction for these potentials because the $4s$ and $4p$ pseudo-wave-functions have their peaks at much larger r than the range of $\Delta^{\text{small } r}(r)$. Hence, for $Z_c=2$, $Z_c=10$, and $Z_c=28$, we use

$$V_T(r)-V_V(r)^{\text{fit}}=-(Z_c/r)\exp(-C_3r)+\Delta^{\text{large } r}(r) \tag{24}$$

and

$$V_T(r)-V_V(r)^{\text{fit}}=-(Z_c/r)\exp(-C_3r)+\Delta^{\text{large } r}(r)+\Delta^{\text{small } r}(r) \tag{25}$$

for $Z_c=18$. For completeness, the Ga to Br potentials with $3d$ in the valence and potentials for the $4d$ with $3d$ in the core are given in the Appendix.

In the work of Andreoni and co-workers,[8] the following expression for V_{ps}^l was assumed:

$$V_{\text{ps}}^l(r)=[(\delta L)/2r^2]\exp(-\gamma r), \tag{26}$$

where both δL and γ are l dependent. For valence states with no core state of the same symmetry, e.g., the p state of the Li-Ne row, negative (δL)'s are required. The same effect is evident in the simpler potential of Simons and Bloch.[5] In our form, it is very apparent why V_{ps}^l is attractive; in that case, the Pauli term, $U_l(r)$, is identically zero, leaving

$$V_{\text{ps}}^l=V_T(r)-V_V(r) \tag{27}$$

which is attractive. The effect of the core states of different symmetries on this pseudovalence state is only the electrostatic screening. The ionic potential is

$$W_l(r)=V_T(r)-V_V(r)-Z_c/r \tag{28}$$

which has the correct limits: $\lim_{r\to 0}W_l(r)=-Z/r$ and $\lim_{r\to\infty}W_l(r)=-Z_v/r$, while Eq. (26) fails for the former limit.

In the following sections we will describe the method of fitting and the quality of the fits using the following analytic form for $V_{\text{ps},l}^{\text{fit}}(r)$:

$$V_{\text{ps},l}^{\text{fit}}(r)=\frac{C_1^l}{r^2}\exp(-C_2^lr)-\frac{Z_c}{r}\exp(-C_3r)-\frac{C_4C_5}{\pi^2(C_5^2+r^2)^2}+C_6\exp(-C_7r), \tag{29}$$

where C_6 and C_7 are set equal to zero for $Z_c=2$, 10, and 28. We note that the Heine-Abarenkov[9] pseudopotential replaces Eq. (29) by a single l-dependent constant A inside a core of a radius R_l, while the "empty-core" pseudopotential of Aschcroft[10] sets $V_{\text{ps},l}(r)$ to zero, independent of l, inside a core radius R_0. In both these forms, it is assumed that a pseudopotential cancellation between a repulsive Pauli force and the Coulomb attraction takes place leaving a constant net potential which is either zero[10] or nonzero.[9] The present pseudopotential approach does not assume such a cancellation but rather calculates it in the density-functional formalism yielding explicit analytic forms for the nearly canceling terms of Eq. (29). Alternative forms are discussed in Ref. 11.

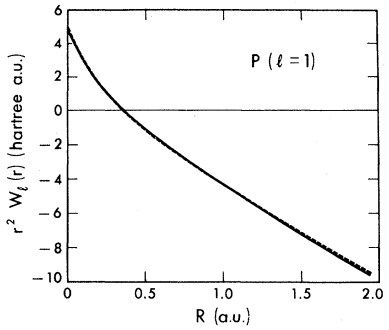

FIG. 5. Setting the weighting function, $\omega(r)$, equal to unity is adequate for states with only one core state. The p potential of phosphorous is used as an example.

II. METHOD OF FITTING

The numerical pseudopotentials are fit with the analytic form expressed in Eq. (29). The fitting parameters are adjusted to minimize the integral,

$$Q \equiv \int_0^\infty (V_{ps,l}^{\text{numerical}} - V_{ps,l}^{\text{fit}})^2 \omega(r) d^3r , \tag{30}$$

i.e., a least-squares fitting with a weighting function, $\omega(r)$. For states with only one core state, choosing $\omega(r)$ to be unity is adequate (See Fig. 5), but as the number of core states increases there is structure in the core region which cannot be fit by this simple form; see Fig. 6. Both R_0^l and R_m^l are not adequately reproduced. One of the objectives of the fitting is to reproduce the trends in the numerical potentials. In order to do this, we choose a weighting function which emphasizes the large-r region. The form for $\omega(r)$ is

$$\omega(r) = \begin{cases} 0, & r < \tilde{R} \\ r^2, & r \geq \tilde{R} . \end{cases} \tag{31}$$

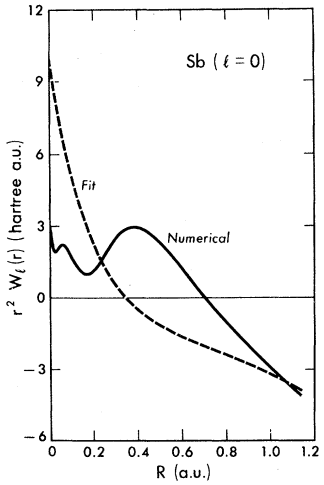

FIG. 6. Simple fitting form for the Pauli term cannot account for the structure in the core region.

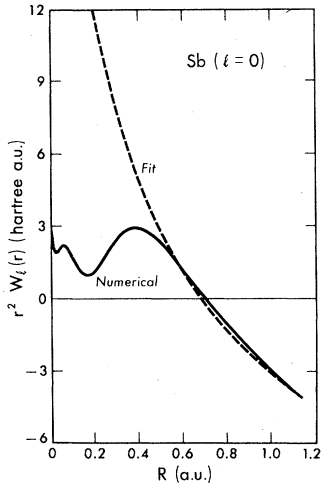

FIG. 7. A weighting function is chosen to ignore the structure in the core and emphasize the large-r region. The resulting fit reproduces R_0 and R_m.

$\tilde{R}$ is chosen to be 0.5 a.u. for both the Na-Ar and K-Kr rows and zero for the Li-Ne row because there is no need to ignore the core region for this row. See Fig. 7 for the fitting with this weighting function.

The local part of the potential, $V_T(r) - V_V(r)$, is fitted first; then, $C_3 - C_7$ are fixed while $V_{ps,l}$ is fitted by C_1^l and C_2^l. The fitting parameters for the first three rows of elements are tabulated in Tables I–IV and are plotted versus Z in Figs. 8(a)–8(g). (See also the Appendix.) The K-Kr row is arbitrarily separated into two rows with $Z_c = 18$ and $Z_c = 28$; from K to Zn, the $3d$ states are treated as valence states while from Ga to Kr the $3d$ is treated as a core state.

III. QUALITY OF THE FITTED POTENTIALS

The value of Q in Eq. (30) is one measure of the quality of the fit; the smaller the Q value the better the fit. However, the true test is how well the

TABLE I. Fitting parameters for the Zunger-Cohen potentials. All energies are in Hartree units.

	$V_T - V_V$			U_l ($l=0$)		U_l ($l=1$)	
$Z_c = 2$	C_3	C_4	C_5	C_1^0	C_2^0	C_1^1	C_2^1
^{3}Li	1.9686	4.7982	5.9880	2.9990	1.0472	0.0	0.0
^{4}Be	2.9456	3.7518	3.1452	3.0169	1.4229	0.0	0.0
^{5}B	3.9668	1.6050	1.8682	3.0315	1.8014	0.0	0.0
^{6}C	5.0062	1.0923	1.4285	3.0731	2.1922	0.0	0.0
^{7}N	6.0734	0.6807	1.1263	3.0487	2.5638	0.0	0.0
^{8}S	6.8700	0.3000	0.5000	3.0500	2.9600	0.0	0.0
^{9}F	7.7131	0.0	0.0	3.0744	3.3609	0.0	0.0
^{10}Ne	8.7366	0.0	0.0	3.0765	3.7456	0.0	0.0

TABLE II. Fitting parameters for the $Z_c=10$ potentials. All energies are in Hartree units.

		V_T-V_V		U_l ($l=0$)		U_l ($l=1$)	
$Z_c=10$	C_3	C_4	C_5	C_1^0	C_2^0	C_1^1	C_2^1
^{11}Na	2.3326	8.7946	1.3053	8.6691	1.354	4.8595	1.0814
^{12}Mg	2.6122	7.1771	3.0945	8.0022	1.4094	4.9062	1.2141
^{13}Al	3.0200	7.1847	2.6178	8.0223	1.5274	4.8883	1.3286
^{14}Si	3.4389	4.3879	1.7767	8.0929	1.6490	4.8731	1.4347
^{15}P	3.8615	7.3943	1.8431	8.3029	1.8115	5.0262	1.6057
^{16}S	4.3209	7.2263	1.5381	8.4635	1.9634	5.1350	1.7581
^{17}Cl	4.8235	7.0678	1.3050	8.6365	2.1205	5.2563	1.9161
^{18}Ar	5.4118	6.8659	1.1078	8.8225	2.2825	5.3928	2.0803

fitted potentials can reproduce the atomic-term values and other features of the all-electron wave function such as the moments, $\langle\psi_{Nl}|r^n|\psi_{Nl}\rangle$. Here ψ_{Nl} is the radial part of the wave function. A comparison between the all-electron moments, $\langle\psi_{Nl}|r^n|\psi_{Nl}\rangle$, and the pseudoelectron moments, $\langle\chi_{Nl}|r^n|\chi_{Nl}\rangle$, determines the similarity between the all-electron wave function and the pseudo-wave-function at different r regions. For $n<0$, the similarity at small r is compared; for $n>0$, the similarity at large r is compared, and for $n=0$, the normalization is checked. In our test, n is an integer between -2 and $+3$, inclusive. In the Zunger-Cohen scheme, the pseudo-wave-function is a linear combination of the all-electron core and valence states [see Eq. (3)]. The all-electron valence state, ψ_{Nl}, can be recovered from χ_{Nl} by core orthogonalization, i.e., subtracting out the core contributions. Let $|\perp\chi_{Nl}\rangle$ denote the core-orthogonalized wave function; it is equal to

$$|\perp\chi_{Nl}\rangle=\left(|\chi_{Nl}\rangle-\sum_c|\psi_{c,l}\rangle\langle\psi_{c,l}|\chi_{Nl}\rangle\right)\Big/\mathfrak{N}\,, \tag{32}$$

where the $|\psi_{c,l}\rangle$'s are the core states and $\mathfrak{N}$ is the normalization constant. With the Zunger-Cohen numerical potentials, the all-electron valence state is fully recovered; χ_{Nl} is given as a linear form in $[\psi_{nl}(r)]$ Eq. (3); hence

$$|\perp\chi_{Nl}\rangle\equiv|\psi_{Nl}\rangle\,, \tag{33}$$

but with the fit potentials, this is not necessarily so because of an imperfect fit. A comparison between $\langle\psi_{Nl}|r^n|\psi_{Nl}\rangle$ and $\langle\perp\chi_{Nl}|r^n|\perp\chi_{Nl}\rangle$ will determine how well the all-electron valence state is recovered. Potentials for the first and last elements of a row are tested. The potentials for the other elements in the row are assumed to be of the same quality.

The atomic-term values calculated with the fitted potential are compared with the all-electron results in Table V. The fitted potentials reproduce the atomic-term values to within 1% to 3%. (The numerical potentials give zero error in the term values.) The pseudoelectron moments are very close to the all-electron moments for $n\geq 0$, and the orthogonalized pseudomoments recover the all-electron results to $\leq 3\%$ (cf. Table VI). The

TABLE III. Fitting parameters for the $Z_c=18$; $l=2$, $C_1^2=C_2^2=0.0$ potentials. All energies are in Hartree units.

			V_T-V_V			U_l ($l=1$)		U_l ($l=1$)	
$Z_c=18$	C_3	C_4	C_5	C_6	C_7	C_1^0	C_2^0	C_1^1	C_2^1
^{19}K	1.5698	15.5520	6.3732	25.682	3.1951	10.615	0.8133	11.078	0.8248
^{20}Ca	1.8822	17.6890	4.3045	29.815	4.1556	11.154	0.8898		
^{21}Sc	2.1414	15.2430	3.6154	28.732	4.4795	11.706	0.9809	11.683	0.9938
^{22}Ti	2.3685	13.7390	3.3310	29.285	4.9331	12.210	1.0726	11.918	1.0802
^{23}V	2.5793	12.8390	3.0885	29.765	5.3572	12.655	1.1619	12.089	1.1621
^{24}Cr	2.7634	6.5083	3.2634	31.525	5.8169	12.781	1.2449	12.260	1.2549
^{25}Mn	2.9744	10.1230	2.7907	32.732	6.2825	13.257	1.3321	12.386	1.3288
^{26}Fe	3.1611	9.2306	2.6890	34.047	6.7046	13.661	1.4247	12.519	1.4112
^{27}Co	3.3435	8.4799	2.6092	35.407	7.1176	13.761	1.4997	12.596	1.4902
^{28}Ni	3.5240	7.7663	2.5226	36.848	7.5357	14.134	1.5925	12.701	1.5714
^{29}Cu	3.6701	4.7710	3.1868	38.370	7.8480	14.230	1.6794	12.845	1.6674
^{30}Zn	3.8772	6.6233	2.3913	39.791	8.3515	14.557	1.7601	12.846	1.7300

TABLE IV. Fitting parameters for the $Z_c=28$ potentials. All energies are in Hartree units.

$Z_c=28$	C_3	V_T-V_V C_4	C_5	U_l ($l=0$) C_1^0	C_2^0	U_l ($l=1$) C_1^1	C_2^1
^{31}Ga	3.3476	16.367	0.911 54	14.934	1.8452	13.115	1.8120
^{32}Ge	3.5107	11.987	0.964 94	14.888	1.8923	12.772	1.8373
^{33}As	3.6166	9.9995	1.345 2	14.954	1.9544	12.779	1.8978
^{34}Se	3.8322	9.9776	1.4135	15.171	2.0278	12.764	1.9577
^{35}Br	4.0707	10.190	1.3565	15.224	2.0910	12.783	2.0218

stability of the numerical potentials against excited configuration was tested in the Zunger-Cohen paper[1]; a similar test is performed for the fitted potential for Ge (see Table VII). The results are very good; eigenvalues are reproduced to $\leq 1\%$.

These analytic potentials, as in the case of the numerical potentials, are "hard-core"; hence, they have non-negligible components for large q in Fourier space. To ensure convergence, one may have to use a very large basis set if plane waves are used. However, if the calculations are performed in real space, there is no convergence problem. Smoothing out the hard-core part of the potential near the origin will improve the convergence; such smoothed potentials seem to give good atomic results.

TABLE V. Tests for the quality of the fitted potentials—reproduction of atomic-term values. Energies are given in eV. AE, fit, Δ, and % denote, respectively, all-electron, fitted potential, error, and percentage error.

			$Z_c=2$			
^{3}Li	ϵ_{2s}		^{10}Ne	ϵ_{2s}	ϵ_{2p}	
AE	−2.149		AE	−34.439	−12.053	
fit	−2.143		fit	−34.365	−11.876	
Δ	+0.006		Δ	+0.075	+0.180	
%	0.3%		%	0.2%	1.5%	
			$Z_c=10$			
^{11}Na	ϵ_{3s}		^{18}Ar	ϵ_{3s}	ϵ_{3p}	
AE	−2.095		AE	−22.655	−9.081	
fit	−2.129		fit	−22.475	−9.054	
Δ	−0.034		Δ	+0.180	+0.027	
%	1.6%		%	0.8%	0.3%	
			$Z_c=18$			
^{19}K	ϵ_{4s}		^{30}Zn	ϵ_{4s}	ϵ_{3d}	
AE	−1.753		AE	−5.042	−9.472	
fit	−1.705		fit	−4.980	−9.528	
Δ	+0.048		Δ	+0.062	−0.056	
%	2.7%		%	1.2%	0.6%	
			$Z_c=28$			
^{31}Ga	ϵ_{4s}	ϵ_{4p}	^{35}Br	ϵ_{4s}	ϵ_{4p}	
AE	−7.912	−1.921	AE	−18.309	−6.833	
fit	−7.835	−1.976	fit	−18.133	−6.829	
Δ	+0.077	−0.055	Δ	+0.177	+0.004	
%	1.0%	2.8%	%	1.0%	0.1%	

IV. TRENDS AND APPLICATIONS

The fitting parameters reflect the chemical trends of the elements. We will examine them in order:

(1) C_1^l [*Fig. 8(a)*]. (a) C_1^l increases as the number of core states increases, indicating a stronger Pauli potential is needed to replace the kinetic energy due to valence-core orthogonality as Z_c increases.

(b) When there is only one core state, e.g., $Z_c=2$ for $l=0$ and $Z_c=10$ for $l=1$, C_1^l is almost a constant. The value of the constant is $2l+3$ (Ref. 1);

TABLE VI. Tests for the quality of the fitted potentials—reproduction of moments. ψ, χ, and $\perp\chi$ denote the all-electron, pseudo- and core-orthogonalized pseudomoments. f is defined as the ratio of the pseudo- (or core-orthogonalized-pseudo) moment to the all-electron moment. Results for Li and Na are tabulated below.

$l=0$	ψ	χ	f	$\perp\chi$	f
			^{3}Li		
$\langle r^{-2}\rangle$	0.4823	0.1222	0.253	0.4857	1.017
$\langle r^{-1}\rangle$	0.3388	0.3069	0.906	0.3399	1.003
$\langle r^{0}\rangle$	1.0000	1.0000	1.000	1.0000	1.000
$\langle r\rangle$	4.1260	4.0650	0.985	4.1180	0.998
$\langle r^{2}\rangle$	20.5300	20.0100	0.975	20.4700	0.997
$\langle r^{3}\rangle$	120.1300	116.6000	0.971	119.7400	0.997
			^{11}Na		
$\langle r^{-2}\rangle$	0.5117	0.1060	0.192	0.5052	0.916
$\langle r^{-1}\rangle$	0.3087	0.2909	0.942	0.3089	1.001
$\langle r^{0}\rangle$	1.0000	1.0000	1.000	1.0000	1.000
$\langle r\rangle$	4.2921	4.2051	0.980	4.2701	0.995
$\langle r^{2}\rangle$	21.9990	21.1720	0.962	21.7250	0.988
$\langle r^{3}\rangle$	131.9550	125.3110	0.950	129.1890	0.979

TABLE VII. Test for the stability of the Ge fitted potential. Energies are given in eV.

$Ge^0 4s^2 4p^2$	ϵ_{4s}	ϵ_{4p}
AE	−10.521	−3.121
fit	−10.429	−3.148
Δ	+0.092	+0.027
%	0.9%	0.9%
$Ge^0 4s^1 4p^3$	ϵ_{4s}	ϵ_{4p}
AE	−11.430	−3.747
fit	−11.339	−3.780
Δ	+0.091	−0.033
%	0.8%	0.9%
$Ge^{+1} 4s^2 4p^1$	ϵ_{4s}	ϵ_{4p}
AE	−18.490	−10.369
fit	−18.569	−10.549
Δ	−0.079	−0.18
%	0.4%	1.7%

this is due to the small-r expansion of χ_{Nl}, $\lim_{r\to 0}\chi_l = a_0 r^{l+2} + \cdots$. As the number of core states increases, there is structure in the core region which is being ignored by our fitting procedure; hence, no such simple relationship exists for C_1^l at higher Z_c.

(c) Although we have arbitrarily divided the third row into $Z_c = 18$ and $Z_c = 28$, with $3d$ in the valence for $Z_c = 18$ and $3d$ in the core for $Z_c = 28$, both C_1^0 and C_1^1 are insensitive to this division because they depend only on the number of core states with $l = 0$ and 1, respectively.

(2) C_2^l [Fig. 8(b)]. (a) C_2^l exhibits an almost linear dependence on Z (or Z_v) for a given Z_c. This can be explained simply. $1/C_2^l$ is a measure of the range of the Pauli potential; thus, it is proportional to the size of the outermost core state of angular momentum l. We denote the size by R_c^l. As Z increases, the nuclear charge pulls the core states inward. Since the potential is $-Z/r$, one expects

$$R_c^l \propto 1/Z . \tag{34}$$

Therefore

$$C_2^l \propto 1/R_c^l \propto Z . \tag{35}$$

Large C_2^l means small core and vice versa. Since Ne has the tightest core, it has the largest C_2.

(b) The discontinuity of C_2 going from lower to higher Z_c is due to the additional core states.

(c) Again, C_2^0 and C_2^1 are insensitive to whether the $3d$ is in the valence or core regions.

(d) As the number of core states for $l = 0$ and $l = 1$ approaches the same value, the nonlocality diminished; e.g., for $Z_c = 18$ and 28, $C_2^0 \simeq C_2^1$.

(3) C_3 [Fig. 8(c)]. (a) $1/C_3$ is the Fermi-Thomas screening length of the core electrons; consequently, it is proportional to the size of the core. The linear relation of C_3 vs Z follows the same argument for C_2^l.

(b) In this case, the distinction between $3d$ in the valence and $3d$ in the core is important because $1/C_3$ is proportional to the size of the whole core. Hence, C_3 jumps to a lower value from Zn to Ga, indicating an increase in core size. However, the change is small since $3d$ is very localized.

(c) If C_3 is approximated by

$$C_3 = a(Z + b) \tag{36}$$

where a and b have different values for different Z_c, the slope indicates the rate at which the core size decreases. A least-squares fit gives

$$C_3 = 0.964(Z - 0.906), \quad Z_c = 2 \tag{37}$$

$$C_3 = 0.443(Z - 6.068), \quad Z_c = 10 \tag{38}$$

$$C_3 = 0.203(Z - 10.571), \quad Z_c = 18 \tag{39}$$

$$C_3 = 0.200(Z - 14.835), \quad Z_c = 28 . \tag{40}$$

The value of the slope decreases as Z_c increases because of screening.

(d) The ratios of the slopes between $Z_c = 2$ and $Z_c = 10$ and between $Z_c = 10$ and $Z_c = 18$ are almost the same:

$$\frac{a(Z_c = 2)}{a(Z_c = 10)} \sim \frac{a(Z_c = 10)}{a(Z_c = 18)} \sim 2.18 . \tag{41}$$

This is an empirical result, and at present, we are unaware of the underlying reason.

Since C_4–C_7 are introduced as a small correction term to the fitted potentials in a particular r region, either large r or small r, their behavior is not as regular as C_1–C_3. Nonetheless, there are some qualitative trends.

The major conclusion from Figs. 8(a)–8(c) is that *at least three parameters* per pseudopotential are required to reproduce the regularities underlying the Periodic Table: one (C_3) for determining the size of the total core, another (C_2) for determining the size of the core due to angular momentum l only, and finally, one (C_1) for determining the strength of the Pauli potential. Furthermore, given the simple forms of C_1, C_2, and C_3 shown in Figs. 8(a)–8(c), each of these can be represented as a linear function of the atomic number Z with two parameters. Hence, for $l = 0$, 1, and 2, a minimum of 12 parameters are needed to represent the (l, Z) dependence of C_1^l and C_2^l. Together with the two (l-independent) parameters for C_3, a minimum of 14 atom-independent parameters are required to reproduce the periodic trends of atomic pseudopotentials. Using the present approach to pseudopotentials, a considerable re-

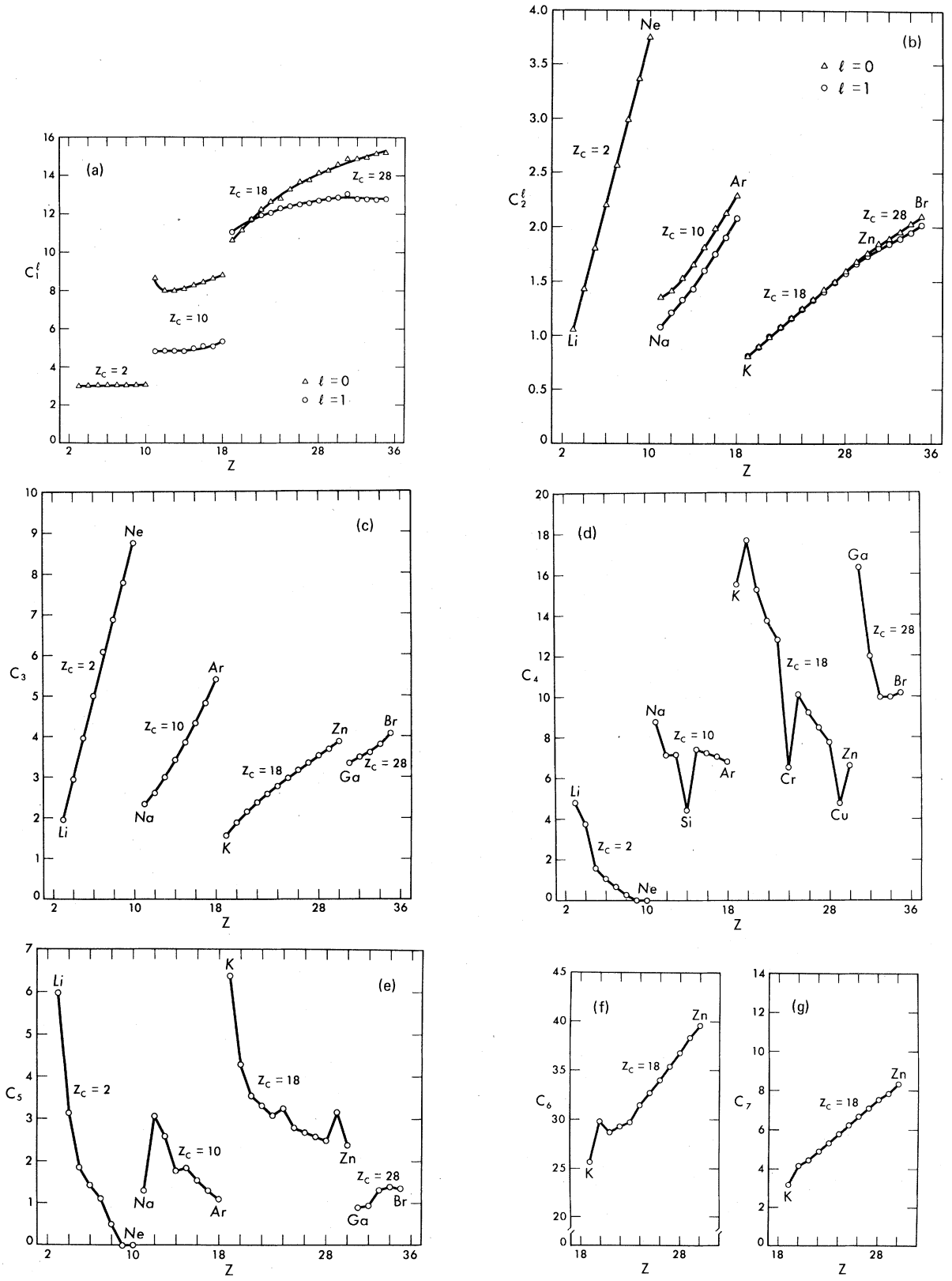

FIG. 8. (a)–(g) Plots of the fitting parameters versus Z, the atomic number.

duction in the number of indispensable degrees of freedom is achieved relative to conventional pseudopotentials to individual atoms or even individual compounds.

(4) C_4 [*Fig. 8(d)*]. (a) C_4 increases with Z_c. C_4 measures the magnitude of the mismatch between ρ_v and n; since the mismatch increases with Z_c, C_4 increases with Z_c.

(b) For $Z_c=2$ and 18, C_4 decreases as Z_v increases. Consider $Z_c=2$; the $2p$ state has no core state; consequently, $\chi_{2p}=\psi_{2p}$ [see Eq. (2)]. The mismatch between ρ_v and n arises from the mismatch between χ_{2s} and ψ_{2s} only. Therefore, as the p state is being populated, the mismatch between ρ_v and n actually decreases, and as a consequence, C_4 decreases. The same regularity exists for the $3d$ series.

(c) The potentials for Si, Cr, and Cu are generated with configurations $3s^23p^13d^1$, $4s^13d^5$, and $4s^13d^{10}$, respectively. The extra occupation of the d state explains the dips of C_4 at Si, Cr, and Cu.

(5) C_5 [*Fig. 8(e)*]. C_5 decreases as Z_v increases. C_5 measures the range of $\Delta^{\text{large } r}(r)$; thus, it should be proportional to the size of the valence state. As Z_v increases, the size of the valence state decreases; therefore, C_5 decreases.

(6) C_6 [*Fig. 8(f)*]. C_6 increases as Z_v increases. $\Delta^{\text{small } r}(r)$ was introduced to account for the core charge accumulated near the origin (see sec. I). C_6 is the magnitude of $\Delta^{\text{small } r}(r)$. As Z_v increases, there is more charge being pulled inward; as a result, C_6 increases.

(7) C_7 [*Fig. 8(g)*]. C_7 increases almost linearly with Z_v. $1/C_7$ is the range of $\Delta^{\text{small } r}(r)$ which is proportional to the core size. Since the core size is inversely proportional to Z_v, C_7 is proportional to Z_v.

Since the quality of the fitted potentials is generally good, we expect that they can be used in place of the numerical potentials for many applications, although *small adjustments in their values may be needed* in view of the approximations made here with respect to the precise Zunger-Cohen pseudopotentials[1] (see Tables V, VI, and VII). In addition, the fitted potentials have other applications because they are analytic, and physical trends can be related to the parameters. If an analytic calculation is performed with these potentials where results can be expressed as functions of the fitting parameters, then the dependence of the calculated quantities on the physical properties of the potential can be revealed. To lowest order when looking for physical trends, the small corrections, $\Delta^{\text{large } r}(r)$ and $\Delta^{\text{small } r}(r)$, can be ignored; therefore, $V_{\text{ps},l}^{\text{fit}}$ has an even simpler form:

$$V_{\text{ps},l}^{\text{fit}} \simeq (C_1^l/r^2)\exp(-C_2^l r) - (Z_c/r)\exp(-C_3 r). \quad (42)$$

Further simplification can be made by fitting C_1^l, C_2^l, and C_3 with functions of Z and Z_c; the pseudopotential can then be completely specified by the atomic-charge and core-charge numbers

$$V_{\text{ps},l}^{\text{fit}} = V_{\text{ps},l}^{\text{fit}}(Z_c, Z; r) \quad (43)$$

and the calculated function of Z and Z_c.

V. CONCLUSION

The Zunger-Cohen first-principles pseudopotentials are successfully fitted with a simple analytic form. This form models the different contributions to the pseudopotential where each contribution is physically relevant. The behavior of the fitting parameters as a function of Z and Z_c is understood in simple physical terms. These analytic pseudopotentials, hopefully, will be useful for determining physical trends in addition to their use for numerical calculations. Note that the underlying density-functional formalism used to derive the present pseudopotentials contains the imperfectly known exchange and correlation energy functional E_{xc}. The deficiencies in the currently known E_{xc} are reflected in systematic discrepancies between the predictions of *any* calculation using this E_{xc} (both pseudopotential and all-electron) and experiment. The parameters in the analytic form of the DF pseudopotential given here may, hence, be slightly modified if one desires to achieve better agreement with experiment.

ACKNOWLEDGMENTS

This work was supported by the National Science Foundation (Grant No. DMR7822465) and by the

TABLE VIII. Ga to Br potentials with $3d$ electrons in the valence.

		V_T-V_V				U_l ($l=0$)		U_l ($l=1$)		U_l ($l=2$)	
$Z_c=18$	C_3	C_4	C_5	C_6	C_7	C_1^0	C_2^0	C_1^1	C_2^1	C_1^2	C_2^2
^{31}Ga	4.1180	7.2615	1.9524	41.691	9.0863	14.546	1.8131	12.736	1.7763	0.0	0.0
^{32}Ge	4.3502	8.5192	1.7789	42.695	9.6643	14.823	1.8874	12.714	1.8323	0.0	0.0
^{33}As	4.6132	9.4193	1.5794	44.105	10.4680	14.885	1.9489	12.717	1.8921	0.0	0.0
^{34}Se	4.9060	10.0720	1.3978	45.845	11.5200	15.162	2.0268	12.757	1.9567	0.0	0.0
^{35}Br	5.2180	10.5920	1.2527	47.618	12.7620	15.269	2.0950	12.824	2.0253	0.0	0.0

TABLE IX. Ga to Br potentials with $3d$ electrons in the core.

	$V_T - V_V$					U_l ($l=0$)		U_l ($l=1$)		U_l ($l=2$)	
$Z_c = 28$	C_3	C_4	C_5	C_6	C_7	C_1^0	C_2^0	C_1^1	C_2^1	C_1^2	C_2^2
^{31}Ga	3.1536	20.4200	0.4616	57.429	5.0386	14.383	1.7930	12.503	1.7437	5.8303	1.2501
^{32}Ge	3.4957	10.5530	0.8724	37.634	9.8418	14.846	1.8855	12.684	1.8228	6.0842	1.3679
^{33}As	3.6439	8.3575	1.0930	47.064	11.7040	14.806	1.9387	12.598	1.8744	6.2339	1.4605
^{34}Se	3.8456	8.0709	1.2267	51.253	13.0870	15.062	2.0150	12.624	1.9378	6.3824	1.5552
^{35}Br	4.0771	8.2950	1.2234	56.430	15.0120	15.161	2.0823	12.689	2.0060	6.5580	1.6541

Division of Materials Sciences, Office of Basic Energy Sciences, U.S. Department of Energy (Grant No. W-7405-ENG-48).

APPENDIX

The definition of *core* and *valence* is rather arbitrary. It is governed only by our chemical intuition and the particular applications. For Ga to Br, we treated the $3d$ electrons as part of the core, but they can also be treated as part of the valence in some applications. Hence, we have also generated the potentials for these elements with the $3d$ electrons in the valence. The fitting parameters are given in Table VIII. With this definition of the valence, the fitting parameters follow the regularities of the K to Zn row. We have also generated potentials for the $4d$ electrons with the $3d$ treated as part of the core. Since the $4d$ orbital is very delocalized in the ground-state configuration, these potentials are generated, for a numerical-stability reason, in the excited configuration where one of the $4p$ electrons is put into the $4d$ state, except for Ga where one of the $4s$ electrons is put into the $4d$ state. The fitting parameters are given in Table IX. Comparison between these parameters with those in Table IV shows that the $l=0$ and $l=1$ potentials are quite independent of the valence configurations. This fact shows that these pseudopotentials depend only on the core, thus implying transferability.

[1]A. Zunger and M. L. Cohen, Phys. Rev. B 18, 5449 (1978).
[2]A. Zunger and M. L. Cohen, Phys. Rev. 41, 53 (1978).
[3]A. Zunger and M. L. Cohen, Phys. Rev. B 19, 568 (1979).
[4]M. H. Cohen and V. Heine, Phys. Rev. 122, 1821 (1961); J. C. Phillips and L. Kleinman, *ibid.* 116, 287 (1959).
[5]G. Simons and A. N. Bloch, Phys. Rev. B 7, 2754 (1972).
[6]The pseudopotentials are derived from a particular reference configuration (usually the ground state).
[7]This choice enforces a minimum anplitude of the pseudo-wave-function in the core region and results in the weakest energy dependence of the pseudopotential (when the pseudo-wave-function is expressed as a combination of DF core plus valence orbitals (Ref. 1). Note that the choice of $\lambda=0$ tested by Zunger and Cohen (Ref. 1) and achieved by including in Eq. (3) more core character than needed just to eliminate the nodes in $\chi_{Nl}(r)$ produces a softer pseudopotential. There is, however, a continuous compromise between the softness of the potential and its energy independence, the limit $\lambda \geq 2$ corresponding to the least energy dependence and the maximum spatial range of similarity between $\chi_{Nl}(r)$ and $\psi_{Nl}(r)$.
[8]W. Andreoni, A. Baldereschi, F. Meloni, and J. C. Phillips, Solid State Common. 25, 245 (1978); J. C. Phillips, Comments Solid State Phys. 9, 11 (1978).
[9]I. V. Abarenkov and V. Heine, Philos. Mag. 12, 529 (1965).
[10]N. W. Ashcroft, Phys. Lett. 23, 48 (1966).
[11]M. L. Cohen and V. Heine, in *Solid State Physics*, edited by H. Ehrenreich, F. Seitz, and D. Turnbull (Academic, New York, 1970), Vol. 24, pp. 37–248.